Conformal Equivalence of Triangle Meshes

Boris Springborn
TU Berlin

Peter Schröder
Caltech

Ulrich Pinkall
TU Berlin

Abstract

We present a new algorithm for conformal mesh parameterization. It is based on a precise notion of *discrete conformal equivalence* for triangle meshes which mimics the notion of conformal equivalence for smooth surfaces. The problem of finding a flat mesh that is discretely conformally equivalent to a given mesh can be solved efficiently by minimizing a convex energy function, whose Hessian turns out to be the well known cot-Laplace operator. This method can also be used to map a surface mesh to a parameter domain which is flat except for isolated cone singularities, and we show how these can be placed automatically in order to reduce the distortion of the parameterization. We present the salient features of the theory and elaborate the algorithms with a number of examples.

Keywords: Discrete Differential Geometry; conformal parameterization; conformal equivalence; discrete Riemannian metric; cone singularities; texture mapping

1 Introduction

In this paper we present a definition for discrete conformal equivalence of triangle meshes and apply it to the problem of conformal mesh parameterization. Our approach arises from two basic premises.

First, the discrete setting should parallel the smooth setting. There the problem of finding a conformal parameterization for a *smooth* surface in space is equivalent to finding a flat metric on the surface that is conformally equivalent to the metric induced by the embedding. Hence, we cast the parameterization problem as one of finding *conformally equivalent flat metrics for a given metric*.

Second, we treat the parameterization problem for *triangle meshes* in the spirit of *Discrete Differential Geometry* [Bobenko and Suris 2005]: instead of viewing discretization as a means of making the smooth problem amenable to numerical methods, we seek to develop on the discrete level a geometric theory that is as rich as the analogous theory for the smooth problem. *The aim is to discretize the whole theory, not just the equations*.

Instead of asking for an *approximation* of the smooth problem, we are thus guided by questions like: What corresponds to a Riemannian metric and Gaussian curvature in an analogous theory for triangle meshes? When should two triangle meshes be considered conformally equivalent? We answer the first question in the obvious way: the edge lengths and the angle defects at vertices. The answer that we give to the second question is also straightforward and intuitive. The striking point is that once we have thus fixed the fundamental definitions of the discrete theory, there is an efficient algorithm to solve the discrete conformal parameterization problem.

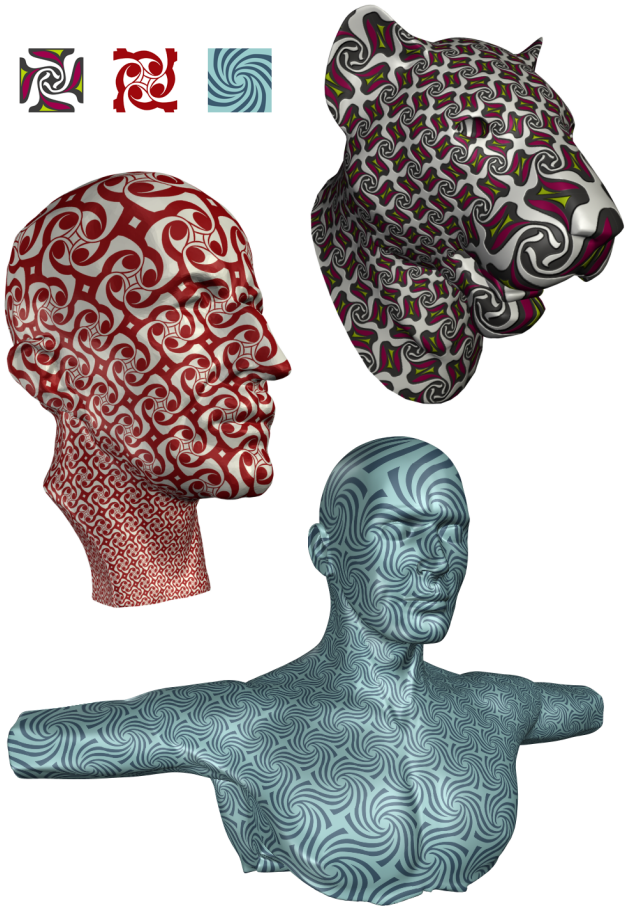

Figure 1: *Customers who visited our Tattoo parlor, where repeating patterns can be applied seamlessly and length distortion is kept low through cone singularities. (Insets show texture tiles.)*

Contributions In this paper we present the first algorithm for mesh parameterization which is based on a definition of *discrete conformal equivalence between triangle meshes* which is satisfactory in the sense that (a) it depends only on the geometry of the meshes and (b) defines an equivalence relation. Meshes in a conformal equivalence class are characterized by length scale factors associated to the vertices and by conserved quantities: the length cross ratios. This discrete notion of conformality comes with a comprehensive theory carrying many of the hallmarks of the smooth setting. Most importantly for graphics applications, we present effective computational procedures based on minimizing a convex energy. The triangulated surfaces may be of arbitrary topology with or without boundary and no a priori cutting is required to deal with higher genus, for example. Flexible boundary conditions support a range of options from full control over boundary curvature to full control over length distortion, including isometrically mapped boundaries. The theory and algorithms also admit cone singularities, which may be placed by the user

or automatically to reduce length distortion and flatten higher genus meshes. Last but not least, our discretely conformal parameterizations admit a piecewise projective interpolation scheme for texture coordinates, which yields improved interpolation at no additional cost.

2 Conformal Equivalence

Our definitions are based on a fairly direct "translation" of classic notions to the discrete setting of meshes. In smooth differential geometry two Riemannian metrics g and $\tilde{g}$ on a differentiable 2-manifold M are said to be *conformally equivalent* if

$$\tilde{g} = e^{2u} g \tag{1}$$

for some smooth function $u : M \to \mathbb{R}$, which gives the logarithm of length change between g and $\tilde{g}$.

In the discrete setting M becomes an abstract surface triangulation consisting of vertices, edges, and triangles, $M = (V, E, T)$. We do not restrict its topology or whether it possesses a boundary. While the combinatorics of a mesh are encoded in such an abstract triangulation, its intrinsic geometry is encoded in the edge lengths. Thus we define:

Definition 2.1. A *discrete metric* on M is a function l on the set of edges E, assigning to each edge e_{ij} a positive number l_{ij} so that the triangle inequalities are satisfied for all triangles $t_{ijk} \in T$.

The smooth function u becomes a function on the set of vertices and we define discrete conformal equivalence as:

Definition 2.2. Two discrete metrics l and $\tilde{l}$ on M are *(discretely) conformally equivalent* if, for some assignment of numbers u_i to the vertices v_i, the metrics are related by

$$\tilde{l}_{ij} = e^{(u_i+u_j)/2} \, l_{ij}. \tag{2}$$

This notion of discrete conformality also appears in [Luo 2004].

It will turn out to be convenient to use the *logarithmic lengths* $\lambda_{ij} := 2 \log l_{ij}$, turning Eq. (2) into the linear relation

$$\tilde{\lambda}_{ij} = \lambda_{ij} + u_i + u_j. \tag{3}$$

Note that this notion of discrete conformal equivalence is indeed an equivalence relation (*i.e.*, it is reflexive, symmetric, and transitive) on the set of discrete metrics on M, and also on the set of meshes. We consider two *meshes* as discretely conformally equivalent if they have the same abstract triangulation and equivalent edge lengths according to Eq. (2).

The primary motivation for this definition is of course the obvious analogy with the smooth setting. Another is that it behaves correctly under Möbius transformations of space: applying a Möbius transformation to the vertices of a mesh, the resulting mesh is discretely conformally equivalent to the untransformed mesh. Möbius transformations—compositions of inversions in spheres—are the only (smooth) conformal transformations of space. Thus, in particular, two meshes whose vertices are related by a smooth conformal transformation of space are also discretely conformally equivalent. (To verify this claim, note that the distance between two points is related to the distance between their image points under a Möbius transformation f by $\|f(x) - f(y)\| = \rho(x)\rho(y)\|x - y\|$ for a real valued function ρ. This is obvious for translations, rotations and scaling, and a straightforward calculation shows that it is true also for inversions in a sphere.) As a practical consequence, this Möbius invariance of discrete conformality enables us to map meshes not only to the plane but also to the sphere.

Discrete conformal equivalence can also be characterized in terms of conserved quantities, namely the length cross ratios:

Definition 2.3. Given a discrete metric l, we associate with each interior edge e_{ij} (between t_{ijk} and t_{jim}) the *length cross ratio*

$$\mathfrak{c}_{ij} := l_{im}/l_{mj} \cdot l_{jk}/l_{ki}. \tag{4}$$

Proposition. *Two meshes are discretely conformally equivalent if and only if their length cross ratios are the same.*

Proof. In one direction, the implication is obvious: if the meshes are discretely conformally equivalent, then their length cross ratios are equal because the scale factors $e^{u/2}$ cancel. To see the converse, consider two discrete metrics l and $\tilde{l}$. We have to show that if their length cross ratios $\mathfrak{c}$ and $\tilde{\mathfrak{c}}$ are equal, then we can associate numbers u_i to the vertices v_i satisfying Eqs. (2) (one equation for each edge). In general, this system of equations for the u_i is overdetermined. For each triangle t_{ijk} the three equations corresponding to its edges already determine values for u at its vertices:

$$e^{u_i} = \tilde{l}_{ij}/l_{ij} \cdot \tilde{l}_{ki}/l_{ki} \cdot l_{jk}/\tilde{l}_{jk}. \tag{5}$$

Considering the neighboring triangle t_{jim} one obtains the same value for e^{u_i} precisely if $\mathfrak{c}_{ij} = \tilde{\mathfrak{c}}_{ij}$. Hence, if l and $\tilde{l}$ have identical length cross ratios, values for u at the vertices are consistently determined by Eqs. (2). □

The discrete theory we have set up now informs our consequent approach. Given a mesh M and a discrete metric l on it, we consider the equivalence class of conformally equivalent metrics. In this class we look for a metric $\tilde{l}$ which is flat. Only in a subsequent step (Section 3.3) do we construct vertex coordinates which realize this flat metric. To find the desired flat metric we need the relation between length and curvature.

2.1 From Curvatures to Lengths

Given a triangle $t_{ijk} \in T$ and lengths l_{ij}, l_{jk}, l_{ki} satisfying the triangle inequality, the angle α^i_{jk} at vertex v_i opposite edge e_{jk} can be recovered by using the cosine formula or the half-angle formula:

$$\alpha^i_{jk} = 2 \tan^{-1} \sqrt{\frac{(l_{ij}+l_{jk}-l_{ki})(l_{jk}+l_{ki}-l_{ij})}{(l_{ki}+l_{ij}-l_{jk})(l_{jk}+l_{ki}+l_{ij})}} \tag{6}$$

(and similarly for $\tilde{\alpha}$ as a function of $\tilde{l}$). Given the angles, curvatures follow as the excess angle sums at vertices. The angle sum at a vertex v_i is denoted by Θ_i:

$$\Theta_i = \sum_{t_{ijk} \ni v_i} \alpha^i_{jk}$$

(and similarly for $\widetilde{\Theta}$). The curvature at an interior vertex is $K_i = 2\pi - \Theta_i$ and the boundary curvature at a boundary vertex is $\kappa_i = \pi - \Theta_i$ (and similarly for $\widetilde{K}$, $\tilde{\kappa}$).

Our goal now is to find a new metric, which is conformally equivalent to a given one, and which possesses prescribed curvatures. Thus, we have to solve the following problem:

Problem. *Given*, for each vertex, a desired angle sum $\widehat{\Theta}_i$, *find* u_i such that the new metric $\tilde{l}$ has angle sums $\widetilde{\Theta}_i = \widehat{\Theta}_i$.

For instance, if we prescribe $\widetilde{\Theta}_i = 2\pi$ at interior vertices, *i.e.*, $\widetilde{K}_i = 0$, a solution to our problem will give a conformally equivalent flat metric with prescribed boundary curvatures $\tilde{\kappa}_i$.

The following conditions on the prescribed angle sums are necessary for the existence of a solution. They must satisfy $0 < \widehat{\Theta} < \pi \cdot |\{t_{ijk} \ni v_i\}|$ because the triangle angles are between 0 and π, and they must be compatible with the Gauss-Bonnet formula

$$\sum_{v_i \in M \setminus \partial M} K_i + \sum_{v_i \in \partial M} \kappa_i = 2\pi\chi(M),$$

where $\chi(M) = |T| - |E| + |V|$ is the Euler characteristic of M.

In view of Eqs. (2) and (6), the problem is equivalent to solving a set of $n := |V|$ equations in n variables u_i. Since the $\widetilde{\Theta}_i$ automatically satisfy one linear relation (Gauss-Bonnet) and the angles are scale invariant, we really have $n-1$ conditions for $n-1$ essential degrees of freedom. We fix the scaling ambiguity by requiring $\sum_{v_i} u_i = 0$.

Luckily, if a solution to this set of non-linear equations exists, it can be found as the *unique minimizer of a convex energy* in u

$$E(u) = \sum_{t_{ijk}\in T} \left(f(\tilde{\lambda}_{ij}, \tilde{\lambda}_{jk}, \tilde{\lambda}_{ki}) - \tfrac{\pi}{2}(u_i+u_j+u_k) \right) + \tfrac{1}{2} \sum_{v_i \in V} \widehat{\Theta}_i u_i \quad (7)$$

where

$$f(\tilde{\lambda}_{ij}, \tilde{\lambda}_{jk}, \tilde{\lambda}_{ki}) = \\ \tfrac{1}{2} \left(\tilde{\alpha}^i_{jk} \tilde{\lambda}_{jk} + \tilde{\alpha}^j_{ki} \tilde{\lambda}_{ki} + \tilde{\alpha}^k_{ij} \tilde{\lambda}_{ij} \right) + \text{Л}(\tilde{\alpha}^i_{jk}) + \text{Л}(\tilde{\alpha}^j_{ki}) + \text{Л}(\tilde{\alpha}^k_{ij}), \quad (8)$$

with $\tilde{\lambda}$ as in Eq. (3); Л(.) denoting Milnor's Lobachevsky function (see Appendix A); and both $\tilde{\lambda}$ and $\tilde{\alpha}$ depending on u.

Indeed, the partial derivatives of this energy are

$$\partial_{u_i} E = \tfrac{1}{2} \left(\widehat{\Theta}_i - \textstyle\sum_{t_{ijk} \ni v_i} \tilde{\alpha}^i_{jk} \right), \quad (9)$$

so that $\operatorname{grad} E(u) = 0$ *iff* u solves the problem. The Hessian of the energy turns out to be one half of the well-known cot-Laplace operator:

$$(\operatorname{Hess} E \cdot \delta u)_i = \tfrac{1}{2} (\Delta \delta u)_i = \tfrac{1}{4} \textstyle\sum_{e_{ij} \ni v_i} w_{ij} (\delta u_i - \delta u_j), \quad (10)$$

with $w_{ij} = \cot \tilde{\alpha}^k_{ij} + \cot \tilde{\alpha}^l_{ij}$ for interior edges and only one cot term for boundary edges. (We adopt the sign convention for the Laplace operator which renders it positive semi-definite. See Appendix B and C for proofs of Eqs. (9) and (10).)

The Hessian is therefore positive semi-definite with only the constant functions in its null-space. This corresponds to the fact that the energy $E(u)$ is scale invariant, *i.e.*, its value does not change if the same number is added to all u_i.

2.2 Relation to Other Approaches

There are many algorithms for mesh parameterization in the literature and we will not attempt a comprehensive review here (the interested reader is referred to [Floater and Hormann 2005] and [Sheffer et al. 2006]). Instead we focus on approaches which are based on *discretized* or *discrete* notions of harmonicity and conformality.

Discrete Harmonicity Discrete versions of the theory of harmonic and analytic functions were developed as early as the 1940s and '50s [Duffin 1956], based on simple difference equations analogous to Laplace's equation and the Cauchy-Riemann equations. Indeed, the discovery of the cot-Laplace operator heralds from this time [Duffin 1959], and these ideas still inform contemporary notions of discrete conformality and harmonicity that are based on linear conditions on the vertex coordinates. Examples of theory and applications include [Pinkall and Polthier 1993; Mercat 2001; Desbrun et al. 2002; Lévy et al. 2002; Gu and Yau 2003; Tong et al. 2007].

The linear theory of discrete harmonicity is interesting and rich, attractive computationally, and enormously useful in applications. But the implied notion of a discretely conformal map as a pair of conjugate discretely harmonic functions is deficient because the inverse of such a map, and the composition of two such maps, are no longer discretely conformal. Thus, this notion of a discretely conformal map does not define a notion of discrete conformal equivalence.

Circle Patterns Going back to an unpublished idea of Thurston (see [Stephenson 2003] for an eyewitness account), discrete conformality can be approached through circle patterns. Here meshes are considered together with a system of circles associated to faces [Kharevych et al. 2006] or vertices [Bowers and Hurdal 2003; Stephenson 2005; Jin et al. 2007; Yang et al. 2008]. Two such meshes are considered conformally equivalent, if the intersection angles of the circles—or inversive distances for non-intersecting circles—are equal in both meshes.

These methods require the solution of non-linear equations, using a convex variational principle, a specially tailored relaxation procedure, or a flow.

This approach to discrete conformality is also not fully satisfactory. In the case of Kharevych *et al.*, the intersection angles determine the curvature of the mesh. Consequently, they must change when the mesh is flattened. For the other circle methods, the notion of discrete conformality either depends on an arbitrary choice of circles, or it is defined only if the edge-lengths satisfy some further conditions, or both.

Curvature Flow Consider u as a function of time and evolving under the negative gradient of E

$$\partial_t u = -2 \operatorname{grad} E = (\widehat{K} - \widetilde{K}) .$$

(For simplicity, assume that M has no boundary.) We may then think of $u^* = \operatorname{argmin}_u E(u)$—which we compute using Newton's method—as the steady state solution of this curvature flow with given target curvatures. Using $\partial_t \widetilde{K} = \partial_u \widetilde{K} \cdot \partial_t u$ together with Eq. (10) we also find that the evolution of the curvature is governed by the equation

$$\partial_t \widetilde{K} = \widetilde{\Delta} (\widehat{K} - \widetilde{K})$$

with $\widetilde{\Delta}$ denoting the (positive semi-definite) cot-Laplace operator of the discrete metric induced by $u(t)$.

In the case where $\widehat{K} = 0$, this flow was considered by Luo [2004] as a discrete version of Yamabe flow. He proves that the flow is variational, but he gives no formula for the energy and does not seem to be aware that the cot-Laplace operator appears in the evolution equation for $\widetilde{K}$. A different discrete curvature flow forms the foundation of the approach of Jin *et al.* [2007] who use Chow and Luo's definition of discrete Ricci flow [2003]. (For 2-dimensional Riemannian manifolds, Yamabe flow is the same as Ricci flow.) Our explicitly variational formulation provides a new approach to discrete Ricci flow for surfaces.

Angle Based Flattening Smooth conformal maps preserve angles exactly. Enforcing this property as-best-as-possible in the discrete setting forms the foundation for Angle Based Flattening (ABF) [Sheffer et al. 2005]. The resulting optimization problem for the angles of the flat mesh is non-linear with non-convex non-linear constraints. It requires sophisticated numerical methods [Sheffer et al. 2005] (for some recent progress see [Zayer et al. 2007]), and is not solved to high enough accuracy to actually produce a flat metric. Thus a further approximation step is necessary to produce the final coordinate functions.

Metric Scaling There is one very recent approach that is closely related to ours [Ben-Chen et al. 2008]. Just as we do, they first compute a metric for the image mesh and only then a set of vertex positions. They start with the following well known relation. Given a smooth 2-manifold and two metrics g, $\tilde{g}$—related through the conformal factor e^{2u} as in Eq. (1)—the curvatures K, $\widetilde{K}$ satisfy:

$$e^{2u} \widetilde{K} = K + \Delta u, \quad (11)$$

where Δ is the—positive semi-definite—Laplace-Beltrami operator. The metric $\tilde{g}$ is flat ($\tilde{K} = 0$), if u solves the Poisson equation

$$\Delta u = -K. \tag{12}$$

To flatten a mesh, Ben-Chen *et al.* proceed by solving the discretized Poisson equation with Δ the cot-Laplace operator in the original metric and K_i the angle defect at a vertex. This is precisely the first Newton step when minimizing our energy $E(u)$. (Their definition of length change induced by the u_i is different from Eq. (2) but this is immaterial to the present argument.) As Ben-Chen *et al.* point out, this does not in general yield a flat metric. They address this by solving a cot-Laplace layout problem in the new metric to find flat vertex positions which approximate the desired metric. In contrast we solve for a (numerically) flat metric and require no further approximation to recover the actual vertex positions.

In their method, target curvatures at the boundary as well as for cone singularities are computed based on a diffusion problem and its associated Green's functions—one each per boundary vertex and interior cone vertex. Incidentally, this computational burden could be removed by using our natural boundary conditions and free cone angles (Sections 4.2 and 5.1).

2.2.1 Discussion

In contrast to all other approaches, ours is based on a proper notion of discrete conformal equivalence for triangle meshes. This notion depends on the meshes alone without any arbitrary choices, and it is adhered to not approximately but precisely.

We have an explicit expression for the energy—as do Kharevych *et al.* but not Jin *et al.*—which facilitates the use of standard, globally convergent, Newton trust region methods. We can also accommodate cone singularities—as introduced by Kharevych *et al.* and recently demonstrated for discrete harmonic approaches [Tong et al. 2007; Kälberer et al. 2007]—and do not require a priori cutting for higher genus surfaces—as is done in ABF. Boundary conditions include constraints on angles or lengths and—novel among all approaches—we support *isometrically* mapped boundaries. Incidentally, the latter also "pick out" the unique least distorted mapping in a given equivalence class (more on these aspects in Section 4).

Comparing our method with ABF illustrates how choosing the "right" discrete notions can lead to concrete practical benefits. ABF preserves triangle angles as much as possible. Our approach preserves the *discrete* conformal structure of the mesh *precisely*. As it happens, this leads to a mathematically simpler optimization problem.

After this discussion of related approaches in computer graphics, we want to acknowledge at least briefly some mathematical work we have built upon. Troyanov [1986] treated the problem of finding a conformally equivalent flat metric with prescribed cone singularities in the smooth setting and proved existence and uniqueness of the solution. The construction of our energy relied heavily on previous work on variational principles for circle patterns [Colin de Verdière 1991; Rivin 1994; Leibon 2002; Bobenko and Springborn 2004]. There is a fruitful connection between all of these circle pattern energies and our energy $E(u)$ on the one side and hyperbolic geometry on the other side. A reader familiar with hyperbolic geometry will realize that the appearance of Milnor's Lobachevsky function is a hint that our energy $E(u)$ has something to do with the volumes of ideal hyperbolic tetrahedra, and she may recognize the logarithmic edge lengths λ_{ij} and length cross ratios $\mathfrak{c}_{ij}$ as Penner coordinates and Thurston-Fock shear coordinates for the Teichmüller spaces $\mathcal{T}_{g,n}$ of genus g Riemann surfaces with n punctures. In fact, minimizing $E(u)$ also solves the problem of finding polyhedral realizations for complete hyperbolic surfaces. But this side of the story is beyond the scope of the present paper.

3 Discretely Conformal Parameterization

Now that the theoretical foundations are laid down we proceed with a discussion of our basic conformal parameterization method.

3.1 Convex Optimization

So far we have a convex energy, but we do not yet have a convex optimization problem since the domain, *i.e.*, the set of u resulting in new edge lengths satisfying the triangle inequalities, is not convex. The inset figure below illustrates the legal range (yellow) of u values for an example triangle. We get around this difficulty by extending the domain of $E(u)$ to all of $\mathbb{R}^n$:

$$\text{if} \quad \tilde{l}_{jk} \not\leq \tilde{l}_{ki} + \tilde{l}_{ij} \quad \text{then} \quad \tilde{\alpha}^i_{jk} = \pi \quad \text{and} \quad \tilde{\alpha}^j_{ki} = \tilde{\alpha}^k_{ij} = 0.$$

Now Eqs. (7) and (8) define $E(u)$ for all values of u. This simple way of extending $E(u)$ is C^1. The gradient of the extended energy is still given by Eq. (9), and the Hessian is given by Eq. (10), where, however, the terms $\cot\tilde{\alpha}^k_{ij}$ in the equation for the weights must be replaced by 0 whenever $\tilde{\alpha}^k_{ij} = 0$ or π. The figure on the right indicates the iso-contours of the extended energy.

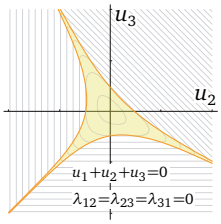

We now have a standard unconstrained convex optimization problem with explicit formulæ for the target function, its gradient, and Hessian. The Hessian is positive semi-definite with only the constant vector in its null-space, reflecting the fact that $E(u)$ remains invariant if a constant vector is added to u. To find the argmin of the extended energy we use the globally convergent Newton-Steihaug trust region method [Steihaug 1983] as implemented in PETSc/TAO [Balay et al. 2007; Benson et al. 2007].

3.2 Violation of the Triangle Inequality

When minimizing the extended energy it is possible that the global minimum is achieved for a u^* giving $\tilde{l}$ which violate the triangle inequality. Figure 2 shows a sampling of such cases which are representative of our experience. In *all* the cases we have observed we found that the triangulation near the bad edge was highly degenerate. In almost all cases this was due to a triangle with one angle close to π. In others, multiple triangles were "folded over" one another (see the second and third example in the top row and first example in the bottom row of Figure 2). Unless the mesh has regions full of such degenerate situations, the problem is simply fixed by flipping or alternatively subdividing the edges opposite the straight angles. Our worst example was the Gargoyle which required flips for 55 out of 74964 edges. (Edge flipping was also considered by Luo [2004], albeit during his curvature flow.)

3.3 Layout

With $u^* = \operatorname{argmin}_u E(u)$ we have new lengths $\tilde{l}$ and angles $\tilde{\alpha}$, but not yet a new mesh. For texture mapping we need vertex positions which requires a layout procedure. Suppose M is a topological disk and there are no cone singularities in the interior. We traverse the dual graph of M in a breadth first manner, laying out opposing vertices each time an edge is crossed. The orientation of each edge is determined by *summation* of corner angles along the traversal. With this layout procedure meshes with 100s of thousands of vertices and length ratios as high as 10^6 can be handled with high precision. Typical examples start with metric

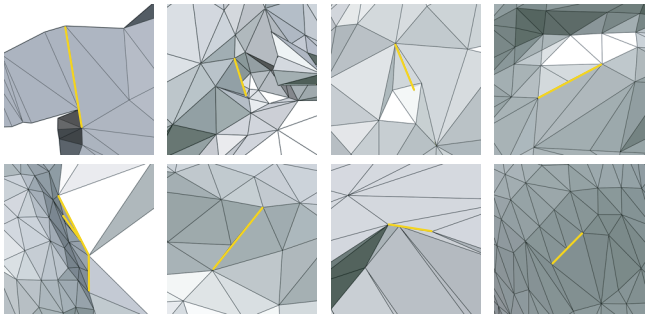

Figure 2: *A sampling of "ripped" edges. In all cases the local geometry was near singular and edge flipping (alternatively, edge subdivision) remedied the trouble.*

data flat to within $\|\operatorname{grad} E(u^*)\|_2 < \epsilon = 10^{-14} \ldots 10^{-12}$ and yield *worst* relative length errors bounded by 10ϵ to 1000ϵ.

Arbitrary topology meshes and those with cone singularities are reduced to the topological disk case. To resolve handles we compute a *system of loops* [Erickson and Whittlesey 2005]. Cutting the loops gives a topological disk, possibly with cones in its interior. To resolve the cones, we trace a path from each cone back to the base vertex of the system of loops using the Dijkstra tree from the first phase. (Any boundaries, including the one due to the system of loops, are treated as if each were a single cone vertex from the point of view of spanning tree construction.) Cutting this cone spanning tree yields a topological disk with no cones in the interior and it may be laid out as above. We have made no efforts to move the paths to inconspicuous locations, though methods such as Seamster [Sheffer and Hart 2002] could be employed. Note that vertices along the cut path will have multiple positions in the layout.

3.4 Piecewise Projective Interpolation

After vertex positions for the image mesh have been found, it is usually necessary, *e.g.*, in texture mapping, to extend the map from the vertices to the whole mesh surface through interpolation. Typically this is done piecewise linearly. For conformally equivalent meshes there is another possibility unique to them.

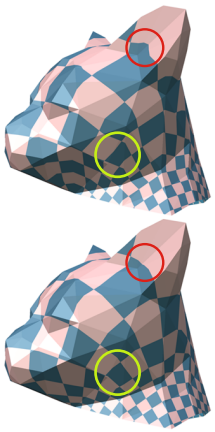

Given a domain and range triangle, there is always a unique projective transformation mapping one onto the other *and* the circumcircle of one onto the circumcircle of the other. In general, these projective mappings do not fit together continuously across edges. A unique exception are the discretely conformally equivalent meshes: This circumcircle preserving piecewise projective interpolation is continuous across edges *iff* the meshes are discretely conformally equivalent. This follows from the proposition in Appendix D, which also shows that in practice it is rather easy to take advantage of this (and we do so in all our texture visualizations): If (x_i, y_i, z_i) and (s_i, t_i) are the vertex coordinates for the original and image mesh respectively, the correct projective interpolation is achieved by performing linear interpolation on the homogeneous coordinates $(x_i, y_i, z_i, 1)$ and $e^{-u_i}(s_i, t_i, 1)$. (Note the scale factor e^{-u_i} which is applied to the homogeneous coordinates of the image mesh.) Since conventional graphics cards support linear interpolation between homogeneous coordinates for texturing anyway, the implementation of the piecewise projective interpolation scheme involves nothing more than using these properly scaled homogeneous coordinates. The figure above shows a comparison between linear interpolation (top) and projective interpolation (bottom) with some notable differences highlighted.

4 Boundary Conditions

Both as a practical matter and as a key to achieving functionality relevant in applications, boundary conditions of different types can be employed. We review these in turn, using practical examples to motivate them.

4.1 Fixed Boundary Curvature

The Problem posed in Section 2.1 requires us to prescribe angle sums $\widehat{\Theta}_i$ for all vertices, *i.e.*, target curvatures $\widetilde{K}_i$ at interior vertices—mostly 0 unless we want a cone singularity—and boundary curvatures $\tilde{\kappa}_i$ for boundary vertices. For example, to achieve a rectangular layout, which has obvious advantages for texture packing, one sets $\widetilde{\Theta}_i = \pi$ for all boundary vertices but four, which receive $\widetilde{\Theta}_i = \pi/2$ (Figure 3, left; see also the Stamp part in Figure 14).

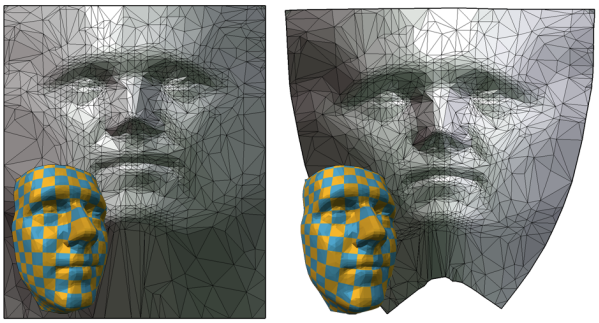

Figure 3: *Fixing curvatures on the boundary can be useful for achieving a particular boundary shape. In contrast, natural boundaries do not constrain the boundary curvature at all (right) and yield the least distorted mapping.*

4.2 Free Boundary Curvature

Alternatively, we may prescribe angle sums $\widehat{\Theta}$ at some vertices and fix u at others. In this case the unique solution can be found by considering the fixed u_i as constants and minimizing $E(u)$ as a function of the remaining variables. Since the value assigned to $\widehat{\Theta}$ at vertices with fixed u is clearly irrelevant for the minimization we may leave it undefined at these vertices. With some u_i fixed, the problem is not scale-invariant anymore and the reduced Hessian becomes positive definite.

An extreme example is to fix u for all boundary vertices. This gives complete control over the length distortion along the boundary while leaving the boundary curvature free.

Natural Boundary Conditions One choice is to set $u_i = 0$ for all boundary vertices. In that case all boundary edges *retain their original length*, *i.e.*, the boundary is mapped *isometrically*. Figure 3 (right) shows a mesh flattened with $\widetilde{\Theta}_i = 2\pi$ for all interior vertices and $u_i = 0$ for all boundary vertices. We call these boundary conditions "natural" because of the following remarkable fact from the smooth theory: Among all flat metrics $\tilde{g}$ that are conformally equivalent to a given metric g, one with *least distortion* is obtained by setting $u = 0$ on the boundary (where the distortion is measured by the Dirichlet energy of u; see Appendix E).

4.3 Topological Spheres

Meshes with sphere topology are sufficiently common that specific parameterization algorithms for them have been designed.

Like Kharevych *et al.* [2006], we exploit the Möbius invariance of discrete conformality to map a mesh to the unit sphere. First some vertex is sent to infinity through inversion. Removing its vertex star we fix $u_i = 0$ for the vertices of its link, and $\widehat{\Theta}_i = 2\pi$ for all other vertices. The resulting planar layout is projected stereographically to the sphere and the knocked out vertex re-inserted at the north pole (Figure 4). Subsequent Möbius normalizations can be applied to ensure, for example, that the center of mass of all vertices is at the origin [Springborn 2005]—a notion of "equidistribution" of points. A simple calculation shows that the resulting mesh is discretely conformally equivalent, even at the knocked out vertex.

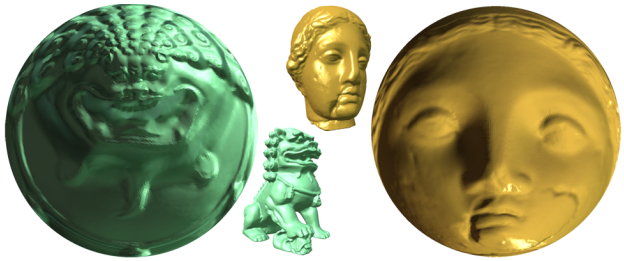

Figure 4: *Sphere parameterizations of Dragon and Hygeia visualized as spheres with the original normals.*

5 Cone Singularities

In practice, a significant issue with conformal maps is their at times severe length distortion. Gu *et al.* [2002], for example, added cuts into the worst distortion area, repeating as necessary. To avoid cutting and the associated discontinuities or complex boundary conditions, Gu and Yau [2003] used topological puncturing and double cover constructions.

The most general and flexible approach to date though was introduced by Kharevych *et al.* [2006] and is based on the selective introduction of isolated vertices which are not required to have zero Gaussian curvature. At these *cone vertices*, the local metric is that of a Euclidean cone with some cone angle $\widetilde{\Theta}_i \neq 2\pi$. This was used both to accommodate higher genus surfaces and reduce length distortion. Placement relied exclusively on human geometric intuition and trial and error. More recently cone singularities

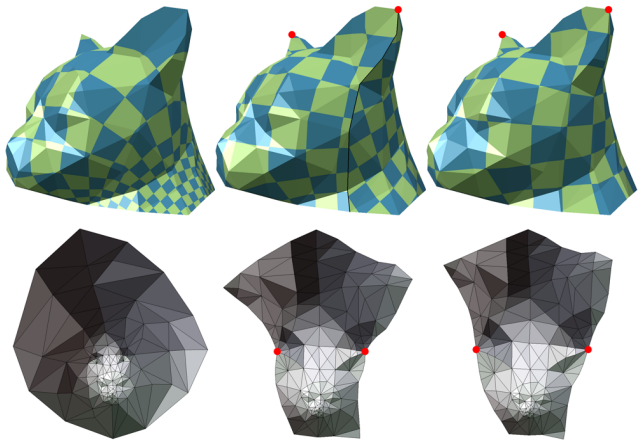

Figure 5: *The effect of cone singularities. Beginning with natural boundary conditions (left), two free cones are added automatically (middle) to reduce distortion (Section 5.1). Depending on the texture, seams may appear. Choosing a suitable cone angle (here π) can remove this problem (right). All three flat metrics are in the same equivalence class as the original metric.*

with cone angles restricted to positive integer multiples of $\pi/2$ were used in rectangular surface patching [Ray et al. 2006] and in discrete harmonic methods [Tong et al. 2007; Kälberer et al. 2007] for the construction of union-of-quad parameterizations. Aiming to align iso-parameter lines (roughly) with principal curvature directions, these approaches all placed cone singularities at numerically estimated umbilic points.

Our method supports free and fixed cone angles (Figure 5) and we are interested in placing cone singularities in a manner which reduces length distortion, *i.e.*, reduces the variation of u, and to do so automatically.

5.1 Automatic Cone Singularities

Where should the zero curvature assumption be relaxed so as to reduce distortion? Considering Eq. (12) for the smooth setting, we see that a local change in K leads to a localized change in u, since adding a Dirac to the right hand side has the effect of adding a Green's function to the solution u. Thus, we choose the vertex with the worst distortion, $v_i = \operatorname{argmax}_{v_i} |u_i|$, as the location for a cone singularity. (If a boundary is present we assume natural boundary conditions, otherwise we set $\sum u_i = 0$.) Instead of prescribing a cone angle, we leave it free, setting $u_i = 0$ (Section 4.2). Since a cone singularity may be seen as the limiting case of a very small hole, this makes sense in view of the minimal distortion property of natural boundary conditions. Our strategy for the *placement* of the cone singularities is thus very similar to the one of Ben-Chen *et al.* [2008], but we do not have to do any extra work to determine the cone angles.

A possible greedy approach starts with some minimizer u of E and selects the vertex with the largest magnitude u_i, setting it to free cone status, and repeating. Figure 6 shows a sequence of such greedy free placements and their impact on u.

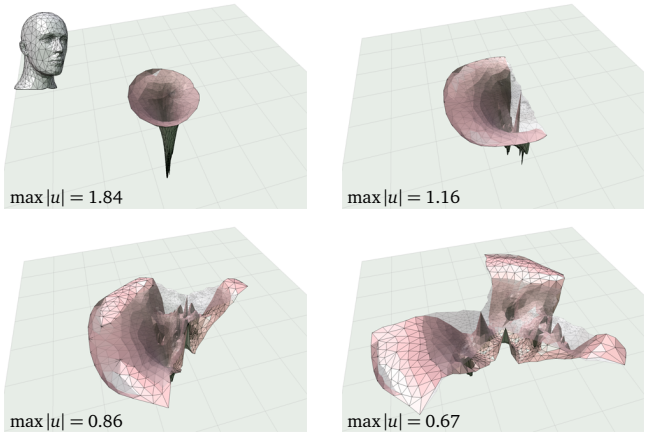

Figure 6: *Visualization of u as a graph over the domain for the mannequin head. Using natural boundaries, zero to three greedy free cones are placed, significantly reducing the magnitude of u in each step.*

If the mesh is a closed surface of genus $\neq 1$ we cannot—due to the Gauss-Bonnet relation—get an initial solution for u without prescribing initial curvatures at vertices. Instead of concentrating all of the required total curvature at some vertex like Ben-Chen *et al.*, we distribute the required total curvature over the whole mesh such that each vertex receives an equal share initially. This is done for the initial solve only. As free cones are placed, the remaining vertices revert to the desired zero curvature setting.

Because the greedy procedure cannot undo earlier decisions, it comes as no surprise that its results can be improved (Figure 7). Four free cone singularities were placed in a greedy manner

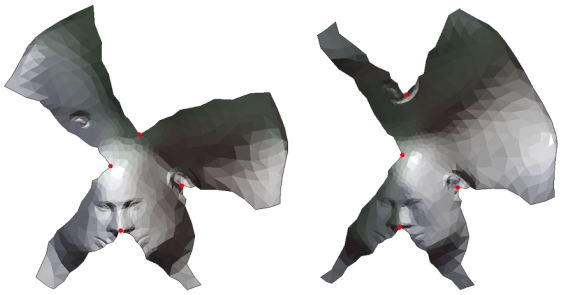

Figure 7: *Comparison of the greedy strategy (left) with concurrent cone optimization (right) for four cones.*

resulting in two cones on top of the head (front and back), at the left ear and on the nose (left). Starting from this initial placement of the four cones, several sweeps—three in this case—of a non-linear Gauss-Seidel solver result in the placement on the right. Cones are now placed far more symmetrically: at the top of the head, on each ear and on the nose. Typically it takes two or three rounds for the cone positions to "settle." To save effort during the Gauss-Seidel stage, we do not solve for u to high accuracy (only one Newton step is used). The final u-function is solved to high precision. Figure 8 shows another where this procedure was applied with a total of 18 cones.

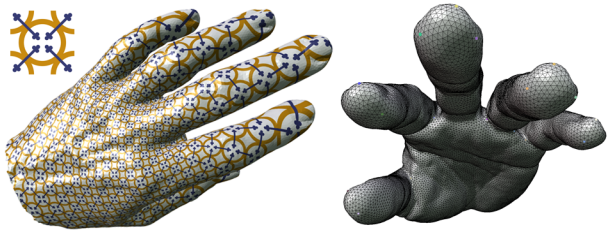

Figure 8: *Olivier's hand with 18 optimized free cones (distributed over the finger tips and inbetween the fingers).*

6 Texture Rectification

When mapping unstructured textures, minimizing distortion in the parameterization is an important criterion. Using textures with symmetries, *e.g.*, checker boards, or when using parameterizations for purposes of resampling, additional constraints on cone placement and cone angles are called for. Quadrilateral patching in particular calls for cones with $\widehat{\Theta}_i = k\pi/2$, $0 < k \neq 4$. A simple example of this is seen in Figure 5, where two free cones were quantized to a fixed angle of π each. Layout followed by a suitable rigid motion and global scale places the two cones at $(0,0)$ and $(1,0)$ in the parameter plane. A seamless checker board texture results.

But quantizing the cone angles to integer multiples of $\pi/2$ is generally not enough if there are more than two cone vertices. Figure 9 illustrates such an example. Four cones of π each were placed on the Venus mesh—a topological sphere. The resulting layout—regardless of the particulars of the cone spanning tree—*must* arrange the cone images as the corners of a parallogram, but generally not as the corners of a rectangle with integer side lengths. In the case of the Venus example a simple shear and scale is enough to produce a seamless checker board texture. (Afterward the metric is no longer conformally equivalent.)

Let us consider this problem in greater generality. Assume M is a topological disk or sphere (the reason for this restriction will be explained below) and any cones multiples of $\pi/2$. For a topological disk, any free cones—resulting from our automatic procedure (Section 5.1)—are rounded to the nearest positive multiple of $\pi/2$. In the case of a closed surface, the quantized

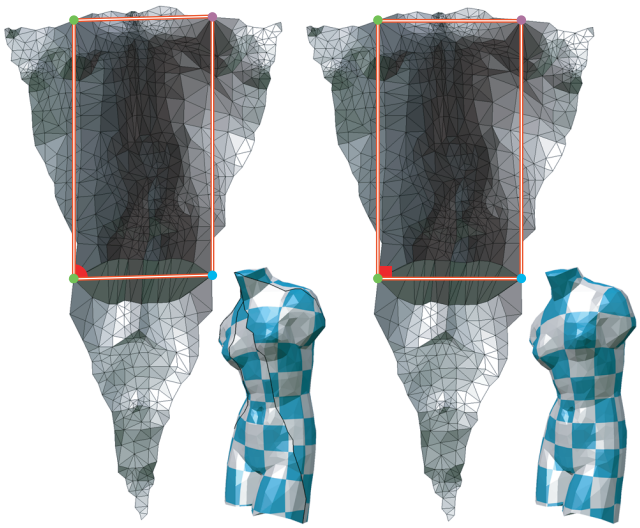

Figure 9: *A layout for the Venus with four cones of π each. These map to corners of a parallelogram (left side). Using a checker board texture leads to artifacts (inset). These can be removed by rectifying the layout with an additional transformation (right side).*

values may violate the Gauss-Bonnet relation, for example, the sum of quantized cone values may be too large. In that case the cone angle that was rounded up the most has its quantized value decreased (unless it is $\pi/2$ already). Repeating this procedure if necessary leads to a set of quantized values which minimize the maximum error between orginal and quantized values while satisfying the Gauss-Bonnet relation. (An analogous procedure can be applied if the initial sum is too small.) Using these now fixed cones the corresponding conformally equivalent metric is solved for and laid out (Section 3.3). It defines the closed *meta-polygon* $P = \{p_i \in \mathbb{C} \,|\, i = 0, \ldots, m-1\}$ given by the vertex positions—treated as complex numbers—of m *special vertices* encountered in a single, ordered traversal of the layout boundary. Special vertices are (1) cone vertices, (2) interior vertices with more than two cut edges incident on them, and (3) boundary vertices with a cut edge incident on them.

Figure 10 shows a meta-polygon for the Lion dataset. Five free cones were placed with the simultaneous optimization procedure, quantized to the nearest multiple of $\pi/2$ ($3\pi/2$ for all five cones in this case), and the corresponding conformally equivalent metric laid out.

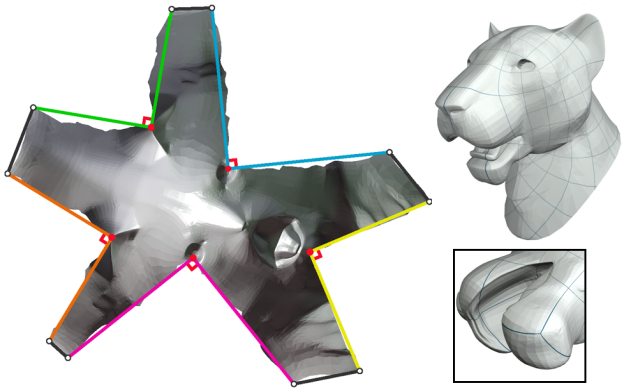

Figure 10: *Meta-polygon for the Lion with quantized cones (solid red) before rectification. After rectification, which forces all cone points to integer locations, the texture tiles the model seamlessly (inset shows $3\pi/2$ cone on chin underside).*

Meta-edges correspond to paths of edges along the boundary of the layout, joining two consecutive special vertices. Such a path is either along the boundary of the original mesh (black edges), or one side of a cut (colored edges), with the other side (matching color) corresponding to a different meta-edge. The two sides of a cut path fit together: a Euclidean motion moves one to the other, and the same motion aligns the corresponding meta-edges. As Figure 10 suggests, the rotation angles of these motions are multiples of $\pi/2$. This is true in general due to the quantized cone angles, but only if the original mesh is simply connected—hence the topological restriction to disks and spheres.

Suppose for a moment that the special vertices of type (1), the cone vertices, have integer coordinates. Then a checkerboard pattern with these vertices in the centers of the squares would fit seamlessly on the mesh, because the Euclidean motions aligning corresponding meta-edges would be symmetries of the pattern.

In reality, the coordinates are not integer. (Figure 11 shows an example with eight optimized and quantized cones, which are not on integers; note the apparent "rip" in the texture on the far end of the right wing.) How close they are to being integer, and hence how much distortion is needed to make them so, depends on rotation and scaling: the larger the scale, the finer the integer grid is relative to the layout size. Suppose such a rotated and scaled layout is given. The idea now is to deform the meta-polygon so that all cone vertices become *complex integers*, $\mathbb{Z}^2 := \mathbb{Z} + I\mathbb{Z} \in \mathbb{C}$, and adapt the layout accordingly. The result will no longer be exactly discretely conformal, but only approximately so: Seamless alignment can *only* be achieved by relaxing the conformality requirement.

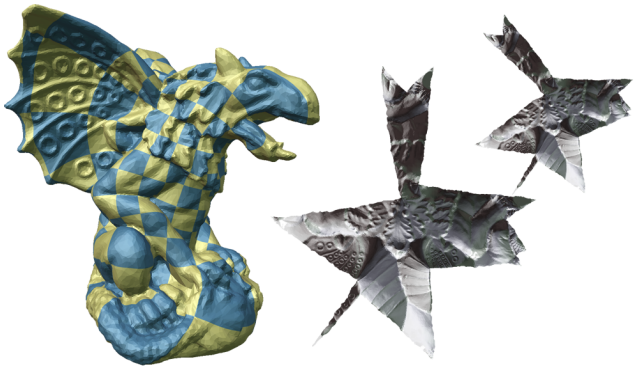

Figure 11: *The Gargoyle—a topological sphere—with eight optimized and subsequently quantized cones. On the top right the optimized cone domain and in the center the result of quantizing the cones. Since the cones do not have integer locations the checkerboard texture has seams.*

6.1 Deforming the Meta-Polygon

When deforming the meta-polygon, associated pairs of meta-edges must maintain their alignment through Euclidean motions with rotations being multiples of $\pi/2$. This requirement is best treated by considering the meta-edge differences $p_{i+1} - p_i =: d_i \in \mathbb{C}$ (all index arithmetic is understood modulo m). Meta-edges due to cutting come in pairs (i, j) and we have

$$d_i = R_{ij} d_j \quad \text{with} \quad R_{ij} \in \{+1, +I, -1, -I\}.$$

The perturbed edge differences $\bar{d}$ must maintain these relations and keep the polygon closed: $\sum \bar{d}_i = 0$. This can be written as

$$A\bar{d} = 0,$$

where A is a matrix with m columns and one more row than there are pairs of corresponding meta-edges. Let N_A be a matrix of (column) basis vectors spanning the null space of A, chosen so that all entries of N_A are complex integers.

Now assume the vertices of the meta-polygon are numbered so that p_0 is a cone vertex and translate it to the origin. Then all cone vertices have integer coordinates if $\sum_{i=0}^{k-1} \bar{d}_i \in \mathbb{Z}^2$ for all k such that p_k is a cone vertex. This can be written as

$$B\bar{d} \in (\mathbb{Z}^2)^l$$

where B is a matrix with m columns and l rows (one less than there are cone vertices). Finally, the columns of BN_A—all entries are complex integers—span a complex subspace which has non-empty intersection with the lattice $(\mathbb{Z}^2)^l$. From this subset lattice we wish to select the nearest (in some norm) lattice point to the cone positions in the given (non-integer) layout. This is an instance of the classic *closest lattice vector* (CLV) problem. Optimal solutions to this problem are computationally hard. For the examples in this paper we proceeded by computing the row rank of BN_A, fixed as many $(l-1)$ of the cones to the nearest point in $\mathbb{Z}^2$ and solved for the remaining (l^{th}) cone location.

Given a solution $\bar{d}$ the implied deformation must now be interpolated across the layout. We do this by performing a cot-Laplace layout as explained in the next section.

6.2 Generalized Laplace Layout

In Section 3.3 we described our breadth first layout procedure to turn metric data into coordinate functions. Another way to turn metric data into coordinate functions is through the use of the cot-Laplace operator.

For a flat metric the cot-Laplace operator—as a map $\mathbb{C}^n \to \mathbb{C}^n$. $(n = |V|)$ and using natural boundary conditions [Desbrun et al. 2002; Lévy et al. 2002]—has a two dimensional (complex) null space consisting of the constant and linear functions on the vertices. The layout procedure produces the unique—up to scale and a rigid motion—null space vector orthogonal to the constant vector. We now turn this prescription around: Given a cot-Laplace operator due to a flat metric, produce the null space vector with zero mean. Because of the presence of cone singularities this cot-Laplace operator must incorporate the edge identifications via rigid motions encoded in the meta-polygon. This is done in the same manner as [Tong et al. 2007]. (Their method accommodates general rotations with no problem including the fact that only a single complex variable is needed for each vertex.) Cone singularities enter as Dirichlet data with positions. The cot-Laplace operator now has only *one* remaining vector in its null space: the original layout (this is true even for general cone angles).

Figure 12: *Rectified domain for Max Planck dataset and visualization of corresponding iso-lines on the mesh.*

We have run comparisons between breadth first and Laplace layout, and found the results to be of comparable accuracy even

for very large layouts. Solving large cot-Laplace systems to high accuracy is in general computationally far more demanding than a simple breadth first traversal, of course.

If the meta-polygon is deformed and we use the *new* cone locations as Dirichlet data the cot-Laplace operator will generally not have a null space anymore and we return the vector of least Dirichlet energy. Figure 12 shows the rectified domain and corresponding iso-lines on the model of Max Planck; see also Figure 10 for the rectified Lion head, and Figure 13 for the rectified Torso parameterization.

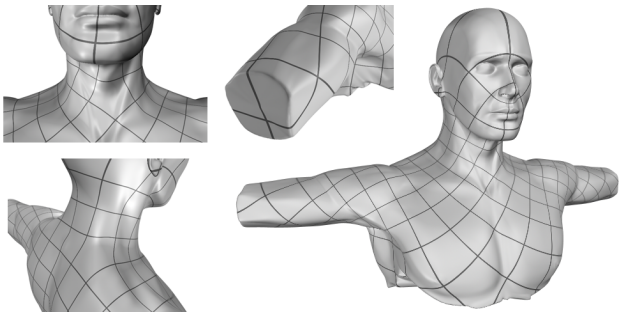

Figure 13: *Visualization of the parameterization on the Torso with 14 optimized, quantized, and subsequently rectified cones (each ear, each nostril, either side of back of neck, on Adam's apple, three on each arm stump and one cone on the torso bottom.*

7 Numerical Results

We have applied our techniques to a number of meshes and report a representative subset of the results here. Mesh sizes ranged from a few hundred vertices to over 200,000 (Julius dataset in Figure 14). In all cases we achieved gradient magnitude residuals in the $10^{-14}\ldots10^{-12}$ range. None of our layouts—either breadth first or the cot-Laplace operator for rectified layouts—have any flipped triangles. The maximum, relative length layout error was always bounded by 10 to 1000 times the gradient residual norm. The Newton trust region solver typically requires around 10 iterations, each iteration having a cost proportional to the assembly and solve phases of a single cot-Laplace problem. The number of Newton steps is thus the relevant figure of merit in terms of overall runtime. (Absolute performance numbers are meaningless since individual solver implementations and processor differences can easily account for factors of 10 and more in observed wall clock times. With this proviso, we note that PETSc/TAO running on a 1.1GHz Pentium M requires 162s for Julius and 230s for the Torso.) The case of the Gargoyle is exceedingly atypical in our experience. This particular mesh is very degenerate in many places and the trust region solver took very small steps. As a quantitative distortion measure we used the area weighted mean of quasi-conformality [Kharevych et al. 2006] (denoted $\|qc\|_1$ in the table), *i.e.*, the ratio of larger to smaller singular value of the surface to parameter plane tangent map. A value of one indicates no angle distortion at all. While it is difficult to compare these numbers across papers ours appear generally somewhat worse than what was reported by Ben-Chen *et al.* and Kharevych *et al.*, for example. Given that we effectively enforce more structure than Ben-Chen and co-workers, and do not allow any approximation of the original data as Kharevych and co-workers do, this is perhaps not surprising. The last column in the table indicates the boundary conditions (free, rectangle, sphere) or the number of optimized (o) free cones, whether they were subsequently quantized (q), and/or rectified (r).

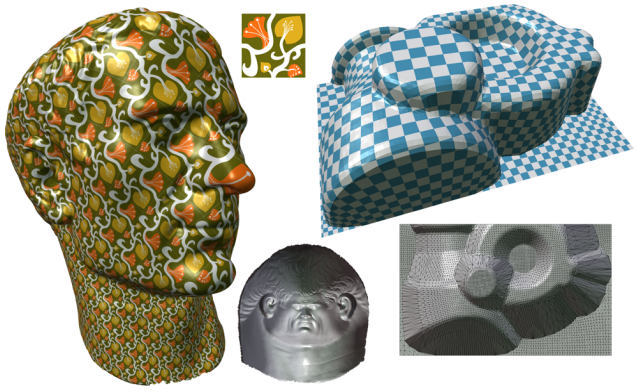

Figure 14: *Further examples of a free boundary (Julius) and use of boundary curvatures to enforce a rectangular domain (Stamp).*

Model	$\|V\|$	Iter.	$\|u\|_{\max}$	$\|qc\|_1$	cones
Face	1042	16	1.164	1.0702	rectangle
Stamp	4100	6	0.431	1.0541	free
Stamp	4100	6	0.742	1.0625	rectangle
Lion	8356	6	1.089	1.0282	5 (oqr)
Olivier	24795	6	1.188	1.0087	18 (o)
Max Planck	25445	11	0.908	1.0097	4 (oqr)
Gargoyle	24990	56	1.849	1.0509	8 (oq)
Hygeia	140654	5	0.650	1.0120	sphere
Torso	142348	12	1.957	1.0048	4 (o)
Torso	142348	21	1.091	1.0036	14 (oqr)
Dragon	152803	5	3.759	1.0277	sphere
Julius	209083	5	1.173	1.0027	free

8 Conclusion

We have shown that our simple notion of discrete conformal equivalence leads to attractive algorithms for mesh flattening, including the automatic determination of cone singularities to reduce distortion and deal with higher genus surfaces, as well as a new piecewise projective interpolation scheme. In Section 6 we have taken first steps to tackle the problem of mapping a symmetric pattern seamlessly onto an arbitrary surface. We have discussed a way to deal with cone singularities, but how to achieve texture rectification for surfaces of higher genus remains an open question. Here we see a promising new direction for further research.

Acknowledgment This work was supported in part by NSF (CCF-0528101 and CCF-0635112), DOE (W-7405-ENG-48/B341492), the Caltech Center for Mathematics of Information, DFG Research Center Matheon, the Alexander von Humboldt Stiftung, and Autodesk. The authors are gratefully indebted to Alexander Bobenko for inspiring discussions. Special thanks to Cici Koenig, Andreas Fabri, Pierre Alliez, and Mathieu Desbrun.

References

Balay, S., Buschelman, K., Eijkhout, V., Gropp, W. D., Kaushik, D., Knepley, M. G., McInnes, L. C., Smith, B. F., and Zhang, H. 2007. PETSc Users Manual. Tech. Rep. ANL-95/11 (Revision 2.3.3), Argonne National Laboratory. http://www.mcs.anl.gov/petsc/.

Ben-Chen, M., Gotsman, C., and Bunin, G. 2008. Conformal Flattening by Curvature Prescription and Metric Scaling. *Comp. Graph. Forum 27*, 2, 449–458.

Benson, S., McInnes, L. C., Moré, J., Munson, T., and Sarich, J. 2007. TAO User Manual. Tech. Rep. ANL/MCS-TM-242 (Revision 1.9), Argonne National Laboratory. http://www.mcs.anl.gov/tao.

Bobenko, A. I., and Springborn, B. A. 2004. Variational Principles for Circle Patterns and Koebe's Theorem. *Trans. Amer. Math. Soc. 356*, 2, 659–689.

Bobenko, A. I., and Suris, Y. B., 2005. Discrete Differential Geometry. Consistency as Integrability. Preprint arXiv:math/0504358v1. To appear in *Graduate Studies in Mathematics* of the AMS.

Bowers, P. L., and Hurdal, M. K. 2003. Planar Conformal Mappings of Piecewise Flat Surfaces. In *Vis. and Math. III*. Springer, 3–34.

Chow, B., and Luo, F. 2003. Combinatorial Ricci Flows on Surfaces. *J. Diff. Geom. 63*, 1, 97–129.

Colin de Verdière, Y. 1991. Un Principe Variationnel pour les Empilements de Cercles. *Invent. Math. 104*, 655–669.

Desbrun, M., Meyer, M., and Alliez, P. 2002. Intrinsic Parameterizations of Surface Meshes. *Comp. Graph. Forum 21*, 3, 209–218.

Duffin, R. J. 1956. Basic Properties of Discrete Analytic Functions. *Duke Math. J. 23*, 335–363.

Duffin, R. 1959. Distributed and Lumped Networks. *J. Math. Mech.* [continued as *Indiana Univ. Math. J.*] *8*, 793–826.

Erickson, J., and Whittlesey, K. 2005. Greedy Optimal Homotopy and Homology Generators. In *Proc. ACM/SIAM Symp. on Disc. Alg.*, SIAM, 1038–1046.

Floater, M. S., and Hormann, K. 2005. Surface Parameterization: a Tutorial and Survey. In *Advances in Multiresolution for Geometric Modelling*, Mathematics and Visualization. Springer, 157–186.

Gu, X., and Yau, S.-T. 2003. Global Conformal Surface Parameterization. In *Proc. Symp. Geom. Proc.*, Eurographics, 127–137.

Gu, X., Gortler, S. J., and Hoppe, H. 2002. Geometry Images. *ACM Trans. Graph. 21*, 3, 355–361.

Jin, M., Kim, J., and Gu, X. D. 2007. Discrete Surface Ricci Flow: Theory and Applications. In *Mathematics of Surfaces 2007*, R. Martin, M. Sabin, and J. Winkler, Eds., Vol. 4647 of *Lecture Notes in Computer Science*. Springer, 209–232.

Kälberer, F., Nieser, M., and Polthier, K. 2007. QuadCover—Surface Parameterization using Branched Coverings. *Comp. Graph. Forum 26*, 3, 375–384.

Kharevych, L., Springborn, B., and Schröder, P. 2006. Discrete Conformal Mappings via Circle Patterns. *ACM Trans. Graph. 25*, 2, 412–438.

Leibon, G. 2002. Characterizing the Delaunay Decompositions of Compact Hyperbolic Surfaces. *Geom. Topol. 6*, 361–391.

Lévy, B., Petitjean, S., Ray, N., and Maillot, J. 2002. Least Squares Conformal Maps for Automatic Texture Atlas Generation. *ACM Trans. Graph. 21*, 3, 362–371.

Lewin, L. 1981. *Polylogarithms and Associated Functions*. North Holland.

Luo, F. 2004. Combinatorial Yamabe Flow on Surfaces. *Commun. Contemp. Math. 6*, 765–780.

Macleod, A. J. 1996. Algorithm 757: MISCFUN, a Software Package to Compute Uncommon Special Functions. *ACM Trans. Math. Softw. 22*, 3, 288–301.

Mercat, C. 2001. Discrete Riemann Surfaces and the Ising Model. *Comm. in Math. Physics 218*, 1, 177–216.

Milnor, J. 1982. Hyperbolic Geometry: The First 150 Years. *Bul. Amer. Math. Soc. 6*, 1, 9–24.

Pinkall, U., and Polthier, K. 1993. Computing Discrete Minimal Surfaces and Their Conjugates. *Experiment. Math. 2*, 1, 15–36.

Ray, N., Li, W. C., Lévy, B., Sheffer, A., and Alliez, P. 2006. Periodic Global Parameterization. *ACM Trans. Graph. 25*, 4, 1460–1485.

Rivin, I. 1994. Euclidean Structures on Simplicial Surfaces and Hyperbolic Volume. *Ann. of Math. (2) 139*, 553–580.

Sheffer, A., and Hart, J. C. 2002. Seamster: Inconspicuous Low-Distortion Texture Seam Layout. In *Proc. IEEE Vis.*, IEEE Comp. Soc., 291–298.

Sheffer, A., Lévy, B., Mogilnitsky, M., and Bogomyakov, A. 2005. ABF++: Fast and Robust Angle Based Flattening. *ACM Trans. Graph. 24*, 2, 311–330.

Sheffer, A., Praun, E., and Rose, K. 2006. Mesh Parameterization Methods and their Applications. *Found. Trends Comput. Graph. Vis. 2*, 2, 105–171.

Springborn, B. 2005. A Unique Representation of Polyhedral Types. Centering via Möbius Transformations. *Math. Z. 249*, 513–517.

Steihaug, T. 1983. The Conjugate Gradient Method and Trust Regions in Large Scale Optimization. *SIAM J. Numer. Anal. 20*, 3, 626–637.

Stephenson, K. 2003. Circle Packing: A Mathematical Tale. *Notices Amer. Math. Soc. 50*, 11, 1376–1388.

Stephenson, K. 2005. *Introduction to Circle Packing*. Cambridge University Press.

Tong, Y., Alliez, P., Cohen-Steiner, D., and Desbrun, M. 2007. Designing Quadrangulations with Discrete Harmonic Forms. In *Proc. Symp. Geom. Proc.*, Eurographics, 201–210.

Troyanov, M. 1986. Les Surfaces Euclidiennes à Singularités Coniques. *Enseign. Math. (2) 32*, 79–94.

Yang, Y., Kim, J., Luo, F., Hu, S., and Gu, D. 2008. Optimal Surface Parameterization Using Inverse Curvature Map. *IEEE Trans. Vis. Comp. Graph.* (to appear).

Zayer, R., Lévy, B., and Seidel, H.-P. 2007. Linear Angle Based Parameterization. In *Proc. Symp. Geom. Proc.*, Eurographics, 135–141.

A Milnor's Lobachevsky Function

Milnor's Lobachevsky function [Milnor 1982] is defined by

$$\Lambda(x) = -\int_0^x \log|2\sin t|\,dt.$$

Up to scale it agrees with *Clausen's integral* $\mathrm{Cl}_2(x) = 2\Lambda(x/2)$ [Lewin 1981]. The function $\Lambda(x)$ is π-periodic, continuous, and odd. It is smooth except at integer multiples of π where its graph has a vertical tangent. For our purposes note that

$$\Lambda'(x) = -\log|2\sin x| \qquad \text{and} \qquad \Lambda''(x) = -\cot x.$$

(For us the absolute value signs are irrelevant because we only consider $\Lambda(\alpha)$ for $0 \le \alpha \le \pi$.) Numerical evaluation can be performed very efficiently and with high accuracy [Macleod 1996].

B Gradient of E

To show Eq. (9) for the partial derivatives of the energy E, we show first that

$$\partial_{\tilde\lambda_{jk}} f(\tilde\lambda_{ij}, \tilde\lambda_{jk}, \tilde\lambda_{ki}) = \tfrac{1}{2}\tilde\alpha^i_{jk}. \tag{13}$$

From Eq. (8) one obtains

$$\begin{aligned}
&\partial_{\tilde\lambda_{jk}} f(\tilde\lambda_{ij}, \tilde\lambda_{jk}, \tilde\lambda_{ki}) = \tfrac{1}{2}\tilde\alpha^i_{jk} + \left(\tfrac{1}{2}\tilde\lambda_{jk} - \log(2\sin\tilde\alpha^i_{jk})\right)\partial_{\tilde\lambda_{jk}}\tilde\alpha^i_{jk} \\
&+ \left(\tfrac{1}{2}\tilde\lambda_{ki} - \log(2\sin\tilde\alpha^j_{ki})\right)\partial_{\tilde\lambda_{jk}}\tilde\alpha^j_{ki} + \left(\tfrac{1}{2}\tilde\lambda_{ij} - \log(2\sin\tilde\alpha^k_{ij})\right)\partial_{\tilde\lambda_{jk}}\tilde\alpha^k_{ij} \\
&= \tfrac{1}{2}\tilde\alpha^i_{jk} + \left(\log\tfrac{\tilde l_{jk}}{2\sin\tilde\alpha^i_{jk}}\right)\partial_{\tilde\lambda_{jk}}\tilde\alpha^i_{jk} + \left(\log\tfrac{\tilde l_{ki}}{2\sin\tilde\alpha^j_{ki}}\right)\partial_{\tilde\lambda_{jk}}\tilde\alpha^j_{ki} + \left(\log\tfrac{\tilde l_{ij}}{2\sin\tilde\alpha^k_{ij}}\right)\partial_{\tilde\lambda_{jk}}\tilde\alpha^k_{ij}.
\end{aligned}$$

Since $\tilde l_{jk}/(2\sin\tilde\alpha^i_{jk}) = \tilde l_{ki}/(2\sin\tilde\alpha^j_{ki}) = \tilde l_{ij}/(2\sin\tilde\alpha^k_{ij}) = \tilde R$ (the circumcircle radius for a triangle with sides $\tilde l_{ij}$, $\tilde l_{jk}$, and $\tilde l_{ki}$) and

$\partial_{\tilde\lambda_{jk}}(\tilde\alpha^i_{jk}+\tilde\alpha^j_{ki}+\tilde\alpha^k_{ij})=0$ (the angle sum is π), Eq. (13) follows. One finds also (in view of Eq. (3)) $\partial_{u_i} f(\tilde\lambda_{ij},\tilde\lambda_{jk},\tilde\lambda_{ki}) = (\partial_{\tilde\lambda_{ij}} + \partial_{\tilde\lambda_{ki}}) f(\tilde\lambda_{ij},\tilde\lambda_{jk},\tilde\lambda_{ki}) = (\tilde\alpha^k_{ij}+\tilde\alpha^j_{ki})/2$, and hence

$$\partial_{u_i}\big(f(\tilde\lambda_{ij},\tilde\lambda_{jk},\tilde\lambda_{ki}) - \tfrac{\pi}{2}(u_i+u_j+u_k)\big) = -\tfrac{1}{2}\tilde\alpha^i_{jk}.$$

Using this, it is straightforward to derive Eq. (9) from Eq. (7).

C Hessian of E

To show Eq. (10) for the Hessian of E, note that $(\mathrm{Hess}\, E\cdot\delta u)_i$ is the derivative of the ith component of $\mathrm{grad}\, E$ in the direction δu. Since

$$(\mathrm{grad}\, E)_i = \tfrac{1}{2}\widehat\Theta_i - \tfrac{1}{2}\sum_{t_{ijk}\ni v_i}\tilde\alpha^i_{jk},$$

and $\widehat\Theta_i$ is constant, we are done once we have shown that the first-order change in $\tilde\alpha^i_{jk}$ is

$$\delta\tilde\alpha^i_{jk} = \tfrac{1}{2}\cot\tilde\alpha^j_{ki}(\delta u_k-\delta u_i)+\tfrac{1}{2}\cot\tilde\alpha^k_{ij}(\delta u_j-\delta u_i). \qquad (14)$$

To derive this relation between $\delta\tilde\alpha$ and δu, we start with the sine theorem: $\tilde l_{ij}/\tilde l_{ki} = \sin\tilde\alpha^k_{ij}/\sin\tilde\alpha^j_{ki}$. (Alternatively one could start with the cosine theorem, compare [Ben-Chen et al. 2008], App. A.) Take the logarithm on both sides to get

$$(\tilde\lambda_{ij}-\tilde\lambda_{ki})/2 = \log\sin\tilde\alpha^k_{ij} - \log\sin\tilde\alpha^j_{ki}$$

and, for the first-order changes,

$$(\delta\tilde\lambda_{ij}-\delta\tilde\lambda_{ki})/2 = \cot\tilde\alpha^k_{ij}\,\delta\tilde\alpha^k_{ij} - \cot\tilde\alpha^j_{ki}\,\delta\tilde\alpha^j_{ki}.$$

Since $\delta\tilde\lambda_{ij}=\delta u_i+\delta u_j$ and $\delta\tilde\lambda_{ki}=\delta u_k+\delta u_i$, one obtains

$$(\delta u_j-\delta u_k)/2 = \cot\tilde\alpha^k_{ij}\,\delta\tilde\alpha^k_{ij} - \cot\tilde\alpha^j_{ki}\,\delta\tilde\alpha^j_{ki},$$

and two other such equations through cyclic permutation of ijk. These three linear equations for $\delta\tilde\alpha^k_{ij}$, $\delta\tilde\alpha^i_{jk}$, $\delta\tilde\alpha^j_{ki}$, are linearly dependent (they sum to zero). Two of them together with $\delta\tilde\alpha^i_{jk}+\delta\tilde\alpha^j_{ki}+\delta\tilde\alpha^k_{ij}=0$ form a linear system of equations which determines $\delta\tilde\alpha$:

$$A\cdot\begin{pmatrix}\delta\tilde\alpha^i_{jk}\\ \delta\tilde\alpha^j_{ki}\\ \delta\tilde\alpha^k_{ij}\end{pmatrix} = \tfrac{1}{2}\begin{pmatrix}\delta u_j-\delta u_i\\ \delta u_i-\delta u_k\\ 0\end{pmatrix}, \qquad A=\begin{pmatrix}\cot\tilde\alpha^i_{jk} & -\cot\tilde\alpha^j_{ki} & 0\\ -\cot\tilde\alpha^i_{jk} & 0 & \cot\tilde\alpha^k_{ij}\\ 1 & 1 & 1\end{pmatrix}.$$

Using the addition theorems for sine and cosine one shows $\det A=-1$. Applying Cramer's rule then yields

$$\delta\tilde\alpha^i_{jk} = -\det\begin{pmatrix}\frac{1}{2}(\delta u_j-\delta u_i) & -\cot\tilde\alpha^j_{ki} & 0\\ \frac{1}{2}(\delta u_i-\delta u_k) & 0 & \cot\tilde\alpha^k_{ij}\\ 0 & 1 & 1\end{pmatrix}$$

which is Eq. (14).

D Circumcircle Preserving Projective Maps

Consider two triangles $\triangle$, $\tilde\triangle$ in the plane with respective Euclidean vertex coordinates $p_i=(x_i,y_i)$ and $\tilde p_i=(\tilde x_i,\tilde y_i)$, and let $l_{ij}=\|p_i-p_j\|$ and $\tilde l_{ij}=\|\tilde p_i-\tilde p_j\|$ be the edge lengths. Define u_i by (5) so that (2) holds. In homogeneous coordinates, p_i and $\tilde p_i$ are represented by the vectors $w_i=(x_i,y_i,1)$ and $\tilde w_i=(\tilde x_i,\tilde y_i,1)$. The projective transformations mapping $\triangle$ to $\tilde\triangle$ come from the linear transformations $f:\mathbb{R}^3\to\mathbb{R}^3$ of homogeneous coordinates with $f(w_i)=a_i\tilde w_i$ where $a_i\in\mathbb{R}_{>0}$.

Proposition. *The projective transformation corresponding to such a linear transformation f maps the circumcircle of $\triangle$ to the circumcircle of $\tilde\triangle$ if and only if a_1, a_2, a_3 are chosen proportional to e^{-u_1}, e^{-u_2}, e^{-u_3}.*

Proof. In homogeneous coordinates $w=(x,y,z)$, the circumcircle of $\triangle$ is described by the equation $q(w)=0$ where $q(w)$ is the quadratic form $q(w)=x^2+y^2+2cxz+2dyz+ez^2$ with c, d, e determined by the conditions $q(w_i)=0$. Similarly, let $\tilde q(\tilde w)$ be the quadratic form describing the circumcircle of $\tilde\triangle$. The circumcircle of $\triangle$ is mapped to the cirumcircle of $\tilde\triangle$ if $q(w)$ is up to some constant factor μ identical to $\tilde q(f(w))$, *i.e.* $q(w)=\mu\cdot\tilde q(f(w))$, or equivalently, if the corresponding symmetric bilinear forms $b(w,w')$, $\tilde b(\tilde w,\tilde w')$ satisfy $b(w,w')=\mu\cdot\tilde b(f(w),f(w'))$. This is the case *iff* $b(w_i,w_j)=\mu\cdot\tilde b(a_i\tilde w_i,a_j\tilde w_j)$, because the w_i form a basis for $\mathbb{R}^3$. But since

$$l_{ij}^2 = q(w_i-w_j) = q(w_i)-2b(w_i,w_j)+q(w_j) = -2b(w_i,w_j)$$

and similarly $\tilde l_{ij}^2=-2\tilde b(w_i,w_j)$, this is equivalent to $l_{ij}^2=\mu\,a_ia_j\tilde l_{ij}^2$, and, using (2), to $a_i=\mu^{-1/2}e^{-u_i}$. □

E Minimal Distortion

Let M be a smooth connected oriented 2-manifold with boundary, equipped with a Riemannian metric g. If $\tilde g$ is a conformally equivalent metric as in Eq. (1), then the Gaussian curvatures $K,\widetilde K$ of g and $\tilde g$ are related by Eq. (11). Thus, the metric $\tilde g$ is flat if u is a solution of the Poisson equation (12).

Now how can one measure the distortion caused by a conformal change of metric? If u is constant, the new metric differs from the old one only by a global change of scale, which we do not consider as distortion. A reasonable measure for the distortion is therefore the *Dirichlet energy* of u

$$D(u) = \tfrac{1}{2}\int_M du\wedge *du = \tfrac{1}{2}\int_M g(\mathrm{grad}\,u,\mathrm{grad}\,u)\,dA$$

which measures "how much u changes."

Theorem. *Among all conformally equivalent flat metrics $\tilde g$, the ones with least distortion are obtained if u is a solution for the Poisson equation* (12) *with $u|_{\partial M}=const$.*

Note that this measure of distortion is symmetric: Interchanging g and $\tilde g$ does not change the distortion. Note also that different choices for the constant boundary value change the solution $\tilde g$ only by a global scale factor, so one might as well choose $u|_{\partial M}=0$.

To prove the theorem, we proceed as usual in the calculus of variations. Suppose $\tilde g$ is flat and consider a variation of $\tilde g$ within the space of conformally equivalent flat metrics, *i.e.*, a variation $\dot u$ of u with $\Delta\dot u=0$. Then the variation of the Dirichlet energy is

$$\dot D = \int_M g(\mathrm{grad}\,u,\mathrm{grad}\,\dot u)\,dA = \int_{\partial M} u\cdot g(\mathrm{grad}\,\dot u,N)\,ds,$$

where N is the outward pointing unit normal vector field on the boundary. As $\dot u$ ranges over all smooth harmonic functions, $g(\mathrm{grad}\,\dot u,N)$ ranges over all smooth functions $h:\partial M\to\mathbb{R}$ satisfying

$$\int_{\partial M} h\,ds = 0. \qquad (15)$$

Indeed, precisely for all h satisfying (15), there is a harmonic $\dot u$ with $g(\mathrm{grad}\,\dot u,N)=h$ on ∂M: This is just the Neumann boundary value problem for Laplace's equation.

So $\tilde g$ is a critical point of the Dirichlet energy under variations within the space of conformally equivalent flat metrics *iff*

$$\forall h \text{ satisfying Eq. (15)}: \int_{\partial M} u\cdot h\,ds = 0.$$

This is clearly the case if $u|_{\partial M}$ is constant. To complete the argument, suppose that $u|_{\partial M}$ is not constant, so $u(p_1)>u(p_2)$ for some $p_1,p_2\in\partial M$. Then, by continuity, there are neighborhoods U_1,U_2 of p_1 and p_2 such that $u(q_1)>u(q_2)$ for all $q_1\in U_1$ and $q_2\in U_2$. Finally, consider a bump function h which is positive only inside U_1, negative only inside U_2, and zero everywhere else, and which satisfies (15) to see that u cannot be critical.